Multimodal Deep Fusion in Hyperbolic Space for Mild Cognitive Impairment Study

Lu Zhang[1], Saiyang Na[1], Tianming Liu[2], Dajiang Zhu[1], and Junzhou Huang[1(✉)]

[1] Department of Computer Science and Engineering, The University of Texas at Arlington, Arlington, TX 76019, USA
jzhuang@exchange.uta.edu

[2] Department of Computer Science, University of Georgia, Athens, GA 30602, USA

Abstract. Multimodal fusion of different types of neural image data offers an invaluable opportunity to leverage complementary cross-modal information and has greatly advanced our understanding of mild cognitive impairment (MCI), a precursor to Alzheimer's disease (AD). Current multi-modal fusion methods assume that both brain's natural geometry and the related feature embeddings are in Euclidean space. However, recent studies have suggested that non-Euclidean hyperbolic space may provide a more accurate interpretation of brain connectomes than Euclidean space. In light of these findings, we propose a novel graph-based hyperbolic deep model with a learnable topology to integrate the individual structural network with functional information in hyperbolic space for the MCI/NC (normal control) classification task. We comprehensively compared the classification performance of the proposed model with state-of-the-art methods and analyzed the feature representation in hyperbolic space and its Euclidean counterparts. The results demonstrate the superiority of the proposed model in both feature representation and classification performance, highlighting the advantages of using hyperbolic space for multimodal fusion in the study of brain diseases. (Code is available here (https://github.com/nasyxx/MDF-HS).)

Keywords: Hyperbolic Space · Multimodal Fusion · MCI

1 Introduction

Alzheimer's disease (AD) is an irreversible progressive neurodegenerative brain disorder that ranks as the sixth leading cause of death in the United States [2]. While AD cannot currently be prevented or cured once established, early

Supplementary Information The online version contains supplementary material available at https://doi.org/10.1007/978-3-031-43904-9_65.

H. Greenspan et al. (Eds.): MICCAI 2023, LNCS 14224, pp. 674–684, 2023.
https://doi.org/10.1007/978-3-031-43904-9_65

diagnosis and intervention during the mild cognitive impairment (MCI - precursor of AD) stage offer a feasible way for patients to plan for the future. Although the neuropathological mechanism of MCI is not fully understood, accumulating evidence suggests that both structural and functional brain alterations have been found in MCI patients [8]. Consequently, numerous multimodal fusion approaches have been published [10,14,20,22,24,27,29], significantly enhancing our comprehension of MCI and AD. Combining various modalities of brain data through multimodal fusion provides an invaluable chance to exploit complementary cross-modal information. The outstanding outcomes obtained by these multimodal fusion techniques in MCI/AD research highlight the essential importance of integrating multimodal brain networks and comprehending their intricate connections in the investigation of brain disorders.

In the most of existing multimodal fusion methods, Euclidean space is typically assumed as the natural geometry of the brain. As such, both feature embedding and model establishment are conducted in the Euclidean space. However, recent studies have suggested that non-Euclidean hyperbolic space may offer a more accurate interpretation of brain connectomes than Euclidean space [1,28]. For example, [1] studied the navigability properties of structural brain networks across species and found that the Euclidean distance cannot fully explain the structural organization of brain connectomes, while hyperbolic space provides almost perfectly navigable maps of connectomes for all species. Similarly, the research in [28] found that the structure of the human brain remains self-similar (a non-Euclidean property) when the resolution of the network is progressively decreased by hierarchical coarse graining of the anatomical regions. Additionally, in the general AI domain, consistent results have been reported, demonstrating that learning hierarchical representations of graphs is easier in the hyperbolic space due to its curvature and geometrical properties [3,7,15]. These compelling findings raise the question of whether hyperbolic space is a better choice for multimodal fusion in the study of brain diseases.

To answer this question, we propose a novel graph-based hyperbolic deep model to conduct multimodal fusion in hyperbolic space for MCI study. Specifically, we embedded brain functional activities into hyperbolic space, where a hyperbolic graph convolution neural network (HGCN) [7] is developed to integrate structural substrate and functional hyperbolic embeddings. The HGCN takes into two inputs: the topology of the network and the associated node features. The input topology is initialized by the individual structural network and iteratively updated by incorporating the corresponding individual functional hyperbolic features to maximize the classification power between elder normal control (NC) and MCI patients. This results in a learned topology that becomes a deeply hybrid connectome embedded in hyperbolic space, combining both brain structural substrate and functional influences. The associated node features are the functional similarities derived from the functional hyperbolic features. By graph convolution in hyperbolic space, node features are aggregated along the topology and used to conduct MCI/NC classification. In the experiments, we comprehensively evaluate the proposed model from three perspectives: Firstly,

we compared the classification performance of our proposed model with state-of-the-art methods. Secondly, we conducted an ablation study to evaluate the effectiveness of both the hyperbolic feature embedding and the hyperbolic graph convolutional neural network. Finally, we visualized, analyzed, and compared the feature representation in hyperbolic space and its Euclidean counterpart. The proposed model achieves the outstanding classification performance, and the results demonstrate the advantages of using hyperbolic space for multimodal fusion in the study of brain diseases.

2 Related Work

Gromov has demonstrated that hyperbolic spaces are particularly well-suited for representing tree-like structures [13], as they allow for the representation of objects that would require an exponential number of dimensions in Euclidean space in only a polynomial number of dimensions in hyperbolic space, with low distortion. To make full use of the geometric properties of hyperbolic space, novel hyperbolic deep neural networks have been proposed and shown to have superior model compactness and predictive performance when compared to their counterparts in Euclidean space. Pioneering works, such as [6,17], have introduced the concept of graph embeddings in hyperbolic space. Recently, HGNN [15] and HGCN [7] were proposed to build graph neural networks in hyperbolic space and achieved remarkable success in graph-related tasks, including node classification [7], graph classification [15], link prediction [7], and graph embedding [3]. Inspired by these works, we attempted to apply the HGCN to brain multimodal fusion studies. In our work, the topology of the HGCN is learnable and incorporates multimodal information from different modalities.

3 Methods

3.1 Data Description and Preprocessing

We used 209 subjects, comprising 116 individuals from the NC group (60 females, 56 males; 74.26 $\pm$ 8.42 years) and 93 subjects from the MCI group (53 females, 40 males; 74.24 $\pm$ 8.63 years) from ADNI dataset. Each subject has structural MRI (T1-weighted), resting-state fMRI (rs-fMRI), and DTI. We performed standard preprocessing procedures as described in [25,26]. In summary, these steps involved skull removal for all modalities. For rs-fMRI images, we conducted spatial smoothing, slice time correction, temporal pre-whitening, global drift removal, and band-pass filtering (0.01–0.1 Hz) using FMRIB Software Library (FSL) FEAT. As for DTI images, we performed eddy current correction using FSL and fiber tracking using MedINRIA. T1-weighted images were registered to DTI space using FSL FLIRT, followed by segmentation using the FreeSurfer package. Subsequently, the Destrieux Atlas [9] was utilized for ROI labeling, and the brain cortex was partitioned into 148 regions. We calculated the average fMRI signal for each brain region as node features and generated the individual structural network using fiber count.

3.2 Preliminary

The hyperbolic space $\mathbb{H}_K^n$ is a specific type of n-dimension *Riemannian manifold* $(\mathcal{M}, g)$ with a constant negative sectional curvature K [4]. It has some unique properties, such as its exponential growth rate, which makes it useful in areas like geometry, topology, and computer science [18]. In hyperbolic space, isometric hyperbolic models are used to maintain the relationship between points without distorting distances. The hyperbolic space is usually defined via five isometric hyperbolic models [19], among which the n-dimensional Poincaré ball model is frequently used because it provides a more intuitive visualization of hyperbolic space, which can be easier to understand than other models. Therefore, in this work, we align with [7] and build our model upon the Poincaré ball model $\mathbb{B}_K^n$. Existing studies [11,16,21] adopt the Möbius transformations as the non-associative algebraic formalism for hyperbolic geometry. Three basic operations of two elements $\mathbf{x}, \mathbf{y}$ on Poincaré ball model, including addition, scalar multiplication, and matrix-vector multiplication, are defined as:

$$\mathbf{x} \oplus_K \mathbf{y} := \frac{(1 - 2K < \mathbf{x}, \mathbf{y} > -K||\mathbf{y}||^2)\mathbf{x} + (1 + K||\mathbf{x}||^2)\mathbf{y}}{1 - 2K < \mathbf{x}, \mathbf{y} > +K^2||\mathbf{x}||^2||\mathbf{y}||^2} \tag{1}$$

$$r \otimes_K \mathbf{x} = \mathrm{Exp}_{\mathbf{0}}^K(r\mathrm{Log}_{\mathbf{0}}^K(\mathbf{x})) \tag{2}$$

$$M \otimes_K \mathbf{x} = \mathrm{Exp}_{\mathbf{0}}^K(M\mathrm{Log}_{\mathbf{0}}^K(\mathbf{x})) \tag{3}$$

A *manifold* $\mathcal{M}$ of n-dimension is a topological space that is locally Euclidean. For all $\mathbf{x} \in \mathcal{M}$, the *tangent space* $\mathcal{T}_{\mathbf{x}}\mathcal{M}$ at a point $\mathbf{x}$ is the vector space of the same n-dimension as $\mathcal{M}$, containing all tangent vector tangentially pass through $\mathbf{x}$. The *metric tensor* $g_{\mathbf{x}}$ [12] on point $\mathbf{x}$ defines an inner product on the associated tangent space. Accordingly, two mappings are defined to achieve transformation between the Euclidean *tangent space* $\mathcal{T}_{\mathbf{x}}\mathcal{M}$ and hyperbolic space $\mathcal{M}$: **Exponential map** $\mathrm{Exp}_{\mathbf{x}}^K : \mathcal{T}_{\mathbf{x}}\mathcal{M} \to \mathcal{M}$ that maps an arbitrary tangent vector $\mathbf{v} \in \mathcal{T}_{\mathbf{x}}\mathcal{M}$ to $\mathcal{M}$ and **logarithmic map** $\mathrm{Log}_{\mathbf{x}}^K : \mathcal{M} \to \mathcal{T}_{\mathbf{x}}\mathcal{M}$ that maps an arbitrary point $\mathbf{y} \in \mathcal{M}$ to $\mathcal{T}_{\mathbf{x}}\mathcal{M}$:

$$\mathrm{Exp}_{\mathbf{x}}^K(\mathbf{v}) := \mathbf{x} \oplus_K (\tanh(\sqrt{|K|}\lambda_{\mathbf{x}}^K \frac{||\mathbf{v}||}{2} \frac{\mathbf{v}}{\sqrt{K}||\mathbf{v}})) \tag{4}$$

$$\mathrm{Log}_{\mathbf{x}}^K(\mathbf{y}) := \frac{2}{\sqrt{|K|}\lambda_{\mathbf{x}}^K} \tanh^{-1}(\sqrt{|K|}||-\mathbf{x} \oplus_K \mathbf{y}||)\frac{-\mathbf{x} \oplus_K \mathbf{y}}{||-\mathbf{x} \oplus_K \mathbf{y}||} \tag{5}$$

where $\lambda_{\mathbf{x}}^K = \frac{2}{1+K||\mathbf{x}||^2}$ is the conformal factor at point $\mathbf{x}$.

3.3 Functional Profile Learning in Hyperbolic Space

In this work, we aim to learn a disease-related functional profile in the hyperbolic space. To this end, we firstly mapped the averaged functional signal of region i in Euclidean – f_i^E, to hyperbolic space via (4): $f_i^H = \mathrm{Exp}_{\mathbf{0}}^K(f_i^E)$, here we choose point 0, the origin in hyperbolic space to conduct transformation. Then upon

f_i^H, we defined the parameterized functional-pairwise distance between region i and region j in hyperbolic space by a learnable mapping matrix M:

$$\phi(M, f_i^H, f_j^H) = ||M \otimes_K (f_i^H \oplus_K -f_j^H)||_2^2, \forall i, j \in 1..N \tag{6}$$

It is worth noting that (6) is a linear projection. It is inadequate for modeling the distance/similarity of the complicated fMRI signals. To alleviate this issue, we introduced nonlinear projection by applying Gaussian kernel:

$$A_{i,j}^{f^H} = \mathrm{Exp}_0^K(\exp(-\frac{\mathrm{Log}_0^K(\phi(M, f_i^H, f_j^H))}{2\sigma^2})) \tag{7}$$

Here, $A_{i,j}^{f^H} \in \mathbb{B}_K^n$ represents the pairwise functional profile between brain regions i and j in hyperbolic space. σ is the bandwidth parameter of Gaussian kernel and is treated as a hyper-parameter. In the proposed model, M is initialized as identity matrix to avoid introducing any bias and iteratively updated during the training process based on classification results.

3.4 Multimodal Fusion by HGCN

A major goal of this work is to conduct effective multimodal fusion of brain structural and functional data in hyperbolic space for MCI study. To achieve this aim, we combined the learned functional profile with the brain structural network in the hyperbolic space by:

$$\hat{A}^H = I \oplus_K (\theta \otimes_K A^{S^H}) \oplus_K ((1-\theta) \otimes_K A^{f^H}) \tag{8}$$

where I is the identity matrix, A^{S^E} is the original individual structural network calculated by fiber count, and $A^{S^H} = \mathrm{Exp}_0^K(A^{S^E})$ is the hyperbolic counterpart of A^{S^E}. $\theta \in (0, 1)$ is a learnable parameter to control the contributions of structural and functional components in the combined new brain connectome $\hat{A}^H$. In the training process, A^{f^H} and A^{S^H} will be iteratively updated, and disease-related knowledge (from classification) is extracted and passed to functional profile (A^{f^H}) and structural network (A^{S^H}) and then transferred to the new brain connectome $\hat{A}^H$. Next, $\hat{A}^H$ will be used as the new topology along with node features in graph convolution conducted by HGCN.

HGCN performs graph convolution within the hyperbolic space in two steps:

$$\tilde{\mathbf{h}}_i^{(l)} = (\mathbf{W} \otimes_K \mathbf{h}_i^{(l)}) \oplus_K \mathbf{b} \tag{9}$$

$$\mathbf{h}_i^{(l+1)} = \mathrm{Exp}_{\tilde{\mathbf{h}}_i^{(l)}}^K(\sum_j^n A\mathrm{Log}_{\tilde{\mathbf{h}}_i^{(l)}}^K(\tilde{\mathbf{h}}_j^{(l)})) \tag{10}$$

where $\mathbf{h}_i^{(l)}$ is the input of i-th node in the l-th layer, $\mathbf{W} \in \mathbb{R}^{d \times d}$ and $\mathbf{b} \in \mathbb{R}^d$ are the weight and bias of the l-th layer. (9) is the operation of input features and model parameters. After that, for each node i, the feature vector of its neighbors

– $\tilde{\mathbf{h}}_j^{(l)}$, will firstly be mapped to i's local tangent space by $\text{Log}^K_{\tilde{\mathbf{h}}_i^{(l)}}$ to conduct graph convolution with adjacency matrix A, then the results will be mapped back to the hyperbolic space by $\text{Exp}^K_{\tilde{\mathbf{h}}_i^{(l)}}$ and used as the input in next layer in HGCN. In a previous study [26], seven different methods for creating functional connectivity were compared, and it was found that the Pearson correlation coefficient (PCC) outperformed other approaches. Therefore, in our work, the PCC of f_i^H is used as node features ($\mathbf{h}_i^{(1)}$) and $\hat{A}^H$ is used as the adjacency matrix A in Eq. 10.

4 Results

4.1 Experimental Setting

Data Settings. In this study, the entire brain was partitioned into 148 distinct regions using the well-established Destrieux Atlas. Averaged fMRI signals were then calculated for each brain region, and the brain structural network (A^S) was generated for each individual. 5-fold cross-validation was performed using a cohort of 209 individuals, consisting of 116 elder normal control (NC) and 93 MCI patients.

Model Settings. The HGCN model in this work has two layers, wherein the output of each HGCN layer was set to 148 and 296, respectively. These outputs were subsequently combined using a hyperbolic fully connected layer [11] with an output size denoted by C, where C corresponds to the number of classes for classification purposes (in our work, $C = 2$). To optimize the model's parameters, an end-to-end training approach was adopted, and the Xavier initialization scheme was utilized. During the training process, the Riemannian SGD [5] optimizer was applied with a standard learning rate of 1.

Table 1. Classification performance comparison with other state-of-the-art methods. ACC: Accuracy; SPE: Specificity; SEN: Sensitivity; AUC: Area under the ROC Curve.

Study	Modality	NC/MCI	ACC(%)	SEN(%)	SPE(%)	AUC
Fang et al. (2020) [10]	MRI+PET	101/204	88.25	79.74	91.58	0.79
Li et al. (2020) [14]	DTI+rsfMRI	37/36	87.70	88.90	86.50	0.89
Zhou et al. (2021) [29]	MRI+PET	142/82	90.35	88.36	92.56	-
Zhang et al. (2021) [22]	Multi-level MRI	275/162	87.82	87.56	88.84	0.93
Zhang et al. (2021) [23]	DTI+rsfMRI	116/98	92.70	-	89.90	-
Shi et al. (2022) [20]	MRI+PET	52/99	80.73	85.98	70.90	0.79
[23] re-implementation	DTI+rsfMRI	116/93	86.23	78.11	87.74	0.83
Proposed	DTI+rsfMRI	116/93	92.30	83.22	89.99	0.87

4.2 Classification Performance Comparison

We compared the classification performance of our proposed model with other state-of-the-art methods on MCI/NC classification task using multi-modal data and presented the results in Table 1. The feature embedding and model development of all the other studies were conducted in Euclidean space. In addition, some of them employed PET data, which tends to yield higher classification accuracy than MRI-based modalities. However, it is noteworthy that our approach utilized noninvasive DTI/fMRI data and achieved outstanding performance with a classification accuracy of 92.3% for MCI/NC classification. Although study [23] reported a slightly higher accuracy than ours, we sought to eliminate biases arising from factors other than the methods by implementing the methods used in [23] with the same data settings as ours and showed results in the " [23] re-implement" row. Notably, our model outperforming [23] in MCI/NC classification when using the same data setting. It is worth mentioning that the only difference between " [23] re-implement" and our method is the space, suggesting that hyperbolic space is a superior choice for multi-modal fusion in MCI/NC classification.

Table 2. Ablation Study. Acc_b: Best Accuracy; Acc_m: Average accuracy. The best and worst results are highlighted by blue and red, respectively.

Model	Manifold	-K	Acc_b(%)↑	Acc_m(%)↑	SPE(%)↑	SEN(%)↑	AUC↑
GCN	Euclidean	0	86.23	83.47	87.74	78.11	0.8293
GCN	Poincaré	1.4	88.02	85.17	89.44	79.86	0.8465
GCN	Poincaré	1.2	87.43	84.93	89.23	79.59	0.8441
GCN	Poincaré	1.0	87.43	84.93	88.80	80.13	0.8446
GCN	Poincaré	0.8	88.02	85.05	89.23	79.85	0.8454
GCN	Poincaré	0.6	87.43	85.05	89.44	79.60	0.8452
GCN	Poincaré	0.4	87.43	85.05	89.22	79.86	0.8454
HGCN	Poincaré	1.4	89.29	83.96	88.83	78.24	0.8353
HGCN	Poincaré	1.2	89.88	83.60	88.22	78.23	0.8323
HGCN	Poincaré	1.0	89.88	85.49	86.81	79.37	0.8309
HGCN	Poincaré	0.8	88.69	83.61	87.71	78.63	0.8317
HGCN	Poincaré	0.6	92.26	86.96	89.99	83.22	0.8660
HGCN	Poincaré	0.4	89.22	86.13	88.38	83.28	0.8583

4.3 Ablation Study

The proposed model implements both feature embedding and graph neural network establishment in hyperbolic space. We conducted ablation studies to evaluate the impact of the two factors on the classification performance of MCI/NC

classification. In contrast to Euclidean space, where the curvature is a constant 0, hyperbolic space has negative curvature, and we evaluated a range of curvature values from −0.4 to −1.4. The results were summarized in Table 2, with the best and worst performances highlighted in blue and red colors, respectively. The best results were obtained when both feature embedding and graph neural network establishment were implemented in hyperbolic space, while the worst results were observed in the pure Euclidean setting. We found that the hybrid combination of GCN established in Euclidean space with the feature embedding in hyperbolic space achieved better performance compared to the pure Euclidean setting, but in most cases, it performed worse than the pure hyperbolic setting. These findings indicate the superiority of hyperbolic feature embedding and graph neural network over their Euclidean counterparts.

4.4 Feature Representation

To gain further insight into the impact of space choice on feature representation, we visualized the distribution of two distinct feature representations in Euclidean space and hyperbolic space. Firstly, we employed principal component analysis (PCA) to project the high-dimensional input feature vectors from both the Euclidean space and the hyperbolic space onto a two-dimensional space. The resulting visualizations are presented in Fig. 1 (a). Notably, the feature vectors in hyperbolic space exhibited a more uniform distribution, with samples distributed more evenly across the space. In contrast, the feature distribution in Euclidean space was non-uniform, with some samples scattered far away from others (highlighted by purple arrows). These differences highlight the advantages of hyperbolic space for representing diverse and complex relationships of input data. Secondly, we projected the latent feature vectors before the classification layer onto a two-dimensional space and presented the results in Fig. 1 (b). These feature vectors are directly related to the classification performance, and their distribution can have a significant impact on classification accuracy. In the hyperbolic space, it is evident that the feature vectors of the two classes have no overlapping areas, while in the Euclidean space, there is a considerable amount

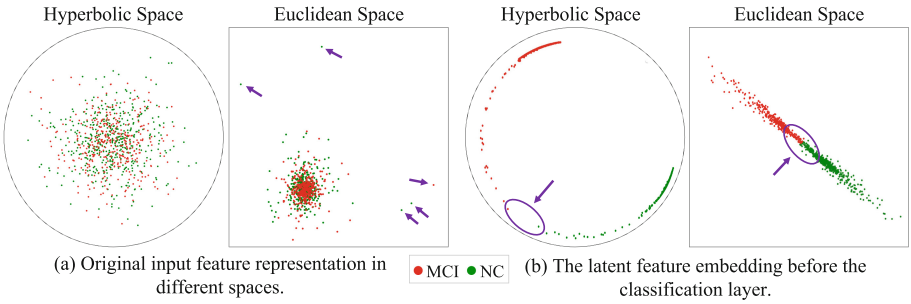

Fig. 1. Distributions of two distinct feature representations in the Euclidean space and the hyperbolic space.

of mixed data where the two types are handed over (highlighted by oval circles). This difference highlights the superiority of hyperbolic space in achieving a clear and distinguishable feature representation for classification tasks.

5 Conclusion

It is widely believed that the AD/MCI related brain alterations involve both brain structure and function. However, effectively modeling the complex relationships between structural and functional data and integrating them at the network level remains a challenge. Recent advances in graph modeling in hyperbolic space have inspired us to integrate multimodal brain networks via graph convolution conducted in the hyperbolic space. To this end, we mapped brain structural and functional features into hyperbolic space and conducted graph convolution by a hyperbolic graph convolution neural network, which enabled us to obtain a new brain connectome that incorporates multimodal information. Our developed model has demonstrated exceptional performance when compared to state-of-the-art methods. Furthermore, the results suggest that feature embedding and graph convolution neural network establishment in hyperbolic space are both crucial for enhancing performance.

Acknowledgement. This work was supported by National Institutes of Health (R01AG075582 and RF1NS128534).

References

1. Allard, A., Serrano, M.Á.: Navigable maps of structural brain networks across species. PLoS Comput. Biol. **16**(2), e1007584 (2020)
2. Association, A.: 2019 Alzheimer's disease facts and figures. Alzheimer's Dementia **15**(3), 321–387 (2019)
3. Bachmann, G., Bécigneul, G., Ganea, O.: Constant curvature graph convolutional networks. In: International Conference on Machine Learning, pp. 486–496. PMLR (2020)
4. Benedetti, R., Petronio, C.: Lectures on hyperbolic geometry. Springer Science & Business Media (1992)
5. Bonnabel, S.: Stochastic gradient descent on Riemannian manifolds. IEEE Trans. Autom. Control **58**(9), 2217–2229 (2013)
6. Chamberlain, B.P., Clough, J., Deisenroth, M.P.: Neural embeddings of graphs in hyperbolic space. arXiv preprint arXiv:1705.10359 (2017)
7. Chami, I., Ying, Z., Ré, C., Leskovec, J.: Hyperbolic graph convolutional neural networks. Adv. Neural Inform. Process. Syst. **32** (2019)
8. Dai, Z., et al.: Disrupted structural and functional brain net-works in Alzheimer's disease. Neurobiol. Aging **75**, 71–82 (2019)
9. Destrieux, C., Fischl, B., Dale, A., Halgren, E.: Automatic parcellation of human cortical gyri and sulci using standard anatomical nomenclature. Neuroimage **53**(1), 1–15 (2010)

10. Fang, X., Liu, Z., Xu, M.: Ensemble of deep convolutional neural networks based multi-modality images for Alzheimer's disease diagnosis. IET Image Proc. **14**(2), 318–326 (2020)
11. Ganea, O., Bécigneul, G., Hofmann, T.: Hyperbolic neural networks. Adv. Neural Inform. Process. Syst. **31** (2018)
12. Greene, R.E.: S. gallot, d. hulin and j. lafontaine, riemannian geometry (1989)
13. Gromov, M.: Hyperbolic groups. In: Gersten, S.M., et al. (eds.) Essays in Group Theory, pp. 75–263. Springer, New York, NY (1987). https://doi.org/10.1007/978-1-4613-9586-7_3
14. Li, Y., Liu, J., Tang, Z., Lei, B.: Deep spatial-temporal feature fusion from adaptive dynamic functional connectivity for mci identification. IEEE Trans. Med. Imaging **39**(9), 2818–2830 (2020)
15. Liu, Q., Nickel, M., Kiela, D.: Hyperbolic graph neural networks. Adv. Neural Inform. Process. Syst. **32** (2019)
16. Mathieu, E., Le Lan, C., Maddison, C.J., Tomioka, R., Teh, Y.W.: Continuous hierarchical representations with poincaré variational auto-encoders. Adv. Neural Informa. Process. Syst. **32** (2019)
17. Muscoloni, A., Thomas, J.M., Ciucci, S., Bianconi, G., Cannistraci, C.V.: Machine learning meets complex networks via coalescent embedding in the hyperbolic space. Nat. Commun. **8**(1), 1615 (2017)
18. Newman, M.E.: Power laws, pareto distributions and Zipf's law. Contemp. Phys. **46**(5), 323–351 (2005)
19. Peng, W., Varanka, T., Mostafa, A., Shi, H., Zhao, G.: Hyperbolic deep neural networks: a survey. IEEE Trans. Pattern Anal. Mach. Intell. **44**(12), 10023–10044 (2021)
20. Shi, Y., et al.: Asmfs: Adaptive-similarity-based multi-modality feature selection for classification of Alzheimer's disease. Pattern Recogn. **126**, 108566 (2022)
21. Shimizu, R., Mukuta, Y., Harada, T.: Hyperbolic neural networks++. arXiv preprint arXiv:2006.08210 (2020)
22. Zhang, J., Zheng, B., Gao, A., Feng, X., Liang, D., Long, X.: A 3D densely connected convolution neural net-work with connection-wise attention mechanism for Alzheimer's disease classification. Magn. Reson. Imaging **78**, 119–126 (2021)
23. Zhang, L., et al.: Roimaging Initiative, A.D.N., et al.: Deep fusion of brain structure-function in mild cognitive impairment. Medical Image Anal. **72**, 102082 (2021)
24. Zhang, L., Wang, L., Zhu, D.: Jointly analyzing Alzheimer's disease related structure-function using deep cross-model attention net-work. In: 2020 IEEE 17th International Symposium on Biomedical Imaging (ISBI), pp. 563–567. IEEE (2020)
25. Zhang, L., Wang, L., Zhu, D.: Recovering brain structural connectivity from functional connectivity via multi-GCN based generative adversarial network. In: Martel, A.L., et al. (eds.) Medical Image Computing and Computer Assisted Intervention – MICCAI 2020: 23rd International Conference, Lima, Peru, October 4–8, 2020, Proceedings, Part VII, pp. 53–61. Springer, Cham (2020). https://doi.org/10.1007/978-3-030-59728-3_6
26. Zhang, L., Wang, L., Zhu, D., Initiative, A.D.N., et al.: Predicting brain structural network using functional connectivity. Med. Image Anal. **79**, 102463 (2022)
27. Zhang, L., Zaman, A., Wang, L., Yan, J., Zhu, D.: A cascaded multi-modality analysis in mild cognitive impairment. In: Suk, H.-I., Liu, M., Yan, P., Lian, C. (eds.) MLMI 2019. LNCS, vol. 11861, pp. 557–565. Springer, Cham (2019). https://doi.org/10.1007/978-3-030-32692-0_64

28. Zheng, M., Allard, A., Hagmann, P., Alemán-Gómez, Y., Serrano, M.Á.: Geometric renormalization unravels self-similarity of the multiscale human connectome. Proc. Natl. Acad. Sci. **117**(33), 20244–20253 (2020)
29. Zhou, P., et al.: Use of a sparse-response deep belief network and extreme learning machine to discriminate Alzheimer's dis-ease, mild cognitive impairment, and normal controls based on amyloid pet/mri images. Front. Med. **7**, 621204 (2021)